Laboratory demonstration of focal plane wavefront sensing using phase diversity: a way to tackle the problem of NCPA in SHARK-NIR. Part II: new characterization tests and alternative wavefront sensing strategies

Daniele Vassallo, Maria Bergomi, Elena Carolo, Davide Greggio, Luca Marafatto, Gabriele Umbriaco, Jacopo Farinato, Andrea Baruffolo, Kalyan Kumar Radhakrishnan Santhakumari, Valentina Viotto, et al.

Laboratory demonstration of focal plane wavefront sensing using phase diversity: a way to tackle the problem of NCPA in SHARK-NIR. Part II: New characterization tests and alternative wavefront sensing strategies

Daniele Vassallo[a,b], Maria Bergomi[a,b], Elena Carolo[a,b], Davide Greggio[a,b], Luca Marafatto[a,b], Gabriele Umbriaco[a,b,c], Jacopo Farinato[a,b], Andrea Baruffolo[a,b], Kalyan Radhakrishnan[a,b], Valentina Viotto[a,b], Jean-Francois Sauvage[d,e], and Thierry Fusco[d,e]

[a]INAF Osservatorio Astronomico di Padova, Vicolo dell'Osservatorio 5, 35122, Padova, Italy
[b]ADaptive Optics National laboratory in Italy (ADONI)
[c]Univ. Padova, Dept. Physics and Astronomy, Vicolo dell'Osservatorio 3, 35122 Padua, Italy
[d]Aix Marseille Univ, CNRS, CNES, LAM, Marseille, France
[e]DOTA, ONERA, Université Paris Saclay, F-91123 Palaiseau, France

ABSTRACT

Phase diversity is a focal-plane wavefront sensing technique. Two or more images of whatever object are required, differing in the amount of a well-calibrated injected aberration (typically a pure defocus). We present here new results concerning the laboratory demonstration of this concept in the specific context of SHARK-NIR, the new-generation high contrast imager for the Large Binocular Telescope. We tested the sensor both on a new dedicated testbed and on the instrument bench itself, which is now fully integrated. We characterized the behavior of the sensor in several conditions, in view of its application to sense SHARK-NIR non-common path aberrations at the telescope. We also investigated some alternative wavefront sensing strategies, such as a curvature-like sensor.

Keywords: wavefront sensing, phase diversity, NCPA, SHARK-NIR, LBT

1. INTRODUCTION

SHARK-NIR[1] is the forthcoming NIR (0.96-1.7µm) XAO (Extreme Adadptive Optics)-fed high-contrast imager for the Large Binocular Telescope (LBT). The instrument has been shipped to LBT at the beginning of June and it is currently undergoing pre-commissioning.[2] It is well known that Non-Common Path Aberrations (NCPA) set the very limit in sensitivity of high contrast observations because of their slow temporal evolution.[3] Therefore, calibrating them, both in the temporal and in the spatial domain, is of paramount importance to achieve the very demanding contrasts requirements for exoplanets detection and characterization.
Phase diversity[4] (PD hereafter), is a wavefront sensing technique whose implementation is of limited opto-mechanical impact because it makes use of focal plane images and only requires a way to introduce a well calibrated aberration (most often a defocus) in the system. This approach has already proven to be successful in sensing NCPA on sky[5] and it has also been validated for implementation in SHARK-NIR with numerical simulations.[6] The first part of characterization tests performed at INAF-Padua laboratories has been presented in a previous publication.[7] For the second part, presented in this work, we set up a new bench with the specific aim of addressing the issues of optimal defocus and optimal number of intra/extra focal images to be used for the reconstruction. In Section 2 we present the optical test bench. Section 3 describes the dataset. In Section 4 we detail the data processing steps and, finally, in Section 5 we report and discuss the results.

Further author information:
Daniele Vassallo: E-mail: daniele.vassallo@inaf.it

2. THE TESTBED

The optical bench is sketched in Figure 1. The main hardware components are a Zygo interferometer (1) and a deformable lens (2). Wavelength is 633nm. The lens (DL hereafter) is an AOL 1816 from Dynamic Optics. A deployable folding mirror (3) sends the light towards the acquisition camera (6), a ZWO ASI183MM (pixel size $2.4\mu m$). The camera is mounted on a motorized linear stage. The imaging lens (5) provides an F\15.6 beam, which means 4 pixels across the PSF. In order to get a sampling closer to SHARK-NIR one, binning 2x2 is required. Binned images can be generated via software, either directly by the camera or a-posteriori from non-binned images.

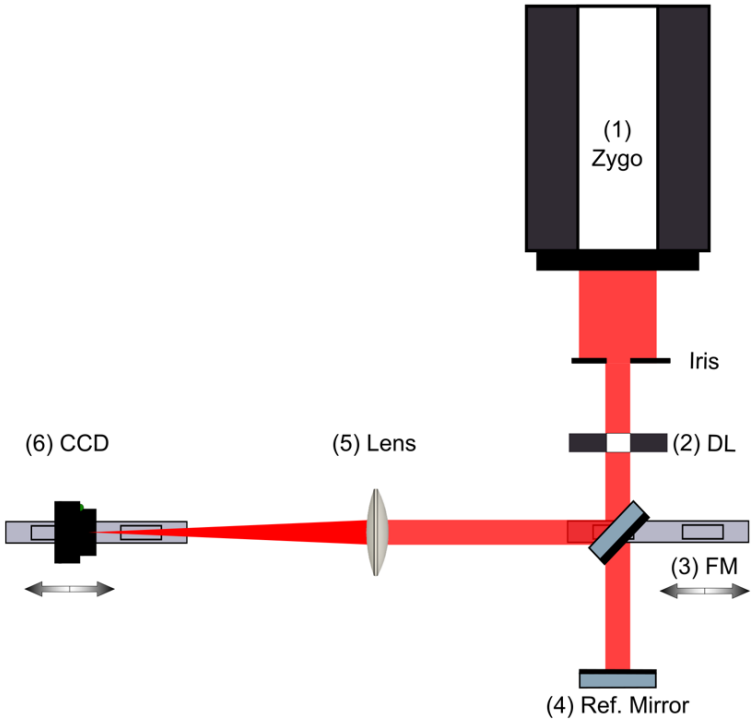

Figure 1. Sketch of the optical bench assembled for the purpose of the tests described in this work.

3. THE DATASET

The capability of the DL to inject Zernike aberrations has been extensively characterized.[8] For the purpose of PD characterization we focused our attention on four composite DL shapes, obtained as combinations of Zernike modes from Z4 up to Z21. For each of these shapes we took a Zygo interferogram, then the set of PD images and finally another Zygo interferogram. Transmitted wavefronts through each of the four DL shapes as measured by Zygo (average of the two interferograms) are shown in Figure 2, while in Figure 3 we report the decompositions in Zernike polynomials. Shape2 generates 116nm RMS of overall aberrations, almost dominated by astigmatism. Shape1 and Shape3 introduce the same amount of aberrations (75nm RMS), but with different modal decompositions. Finally, Shape4 injects only a small amount of aberrations (38nm RMS).
Images for PD were taken at 9 different positions of the camera along the optical axis: 0 (i.e. the best focus position), $\pm 1.233mm$, $\pm 1.849mm$, $\pm 2.464mm$ and $\pm 3.082mm$, corresponding to $\pm 1\lambda$, $\pm 1.5\lambda$, $\pm 2\lambda$ and $\pm 2.5\lambda$ defocus peak-to-valley, respectively. Throughout this paper, we will use the minus sign to identify intra-focal images and the plus sign for extra-focal images. Defocus amplitude is always intended as peak-to-valley, unless otherwise stated. For each camera position we acquired 10 images and 10 darks. All images were acquired without binning, except for Shape4, whose images are binned 2x2 via the camera software and, therefore, non-binned data are not available.

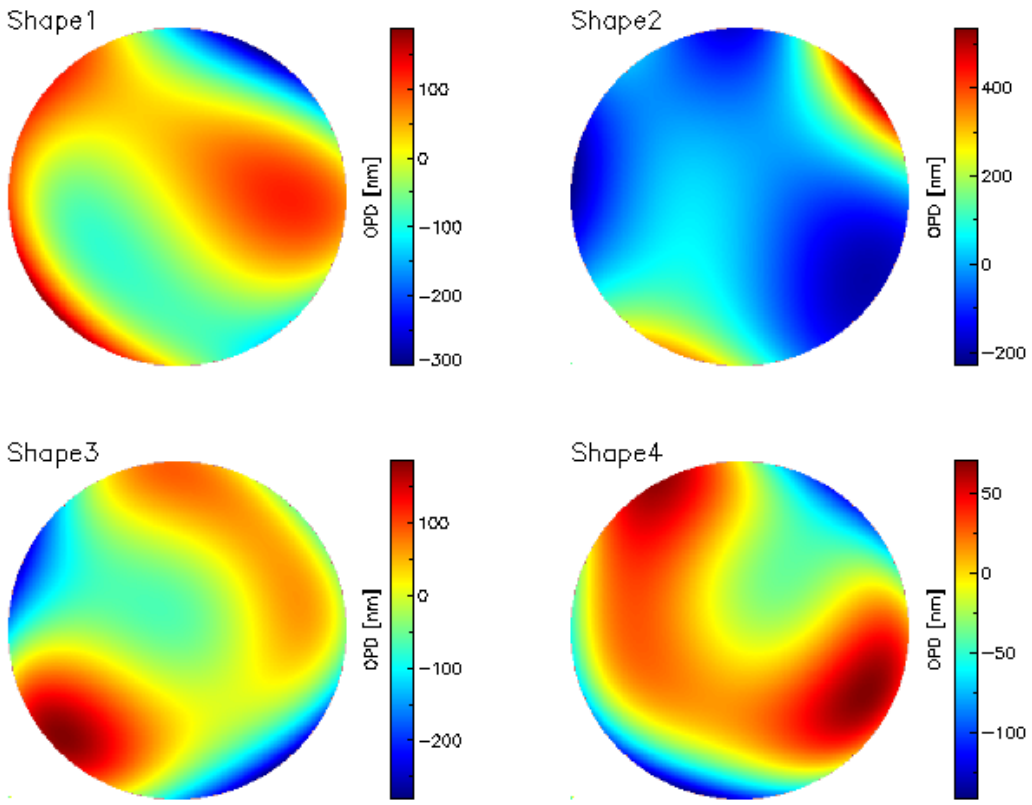

Figure 2. Optical path difference maps as measured by Zygo for each of the four deformable lens composite shapes analyzed in this work.

4. DATA PROCESSING

Pre-processing of raw data taken at each camera position (ten images and ten darks) consists of the following steps: dark-subtraction, image registration, mean-stack and (eventually) binning. Because of bench turbulence, registration of the images before taking the average is recommended in order to get a clean final product. Whereas the images feature a clear central core (e.g. in most of the in-focus images) registration is done by simply measuring the PSF centroids via 2D Gaussian fitting. When a central core is not present, as it happens for the vast majority of the images in the dataset, registration is done by means of a template matching algorithm. However, in some of the images, especially those in which the defocus is small, template matching fails because the signal is distributed over a small amount of pixels and this results in an insufficient amount of features to be used to perform the match. In those cases, images are stacked without registration. As an example, Figure 4 shows the full pre-processed image sequence for Shape3 (no binning).

Pre-processed images are finally given in input to the PD s oftware. The software has been developed by ONERA and it is based on a maximum a-posteriori (MAP) approach[9] for phase retrieval. The software offers very useful features, such as the possibility to estimate, together with the unknown phase (and object), also differential tip/tilt among the input images. This is a crucial feature, since defocus injection most of the times comes with tip/tilt as well. On our testbed, residual alignment error between the camera stage and the optical axis results in peak-to-valley misalignments in the images of the order of several camera pixels. In a similar way, defocus can be optimized by the software as well. This helps mitigating the error on the knowledge of the defocus we are injecting. This is less crucial in our setup, since defocus is known very precisely thanks to the motorized stage. We can refer to the simultaneous optimization of tip, tilt and defocus as "full optimization mode". If not otherwise stated, PD reconstruction is performed in full optimization mode. Moreover, reconstruction is modal up to Zernike 21.

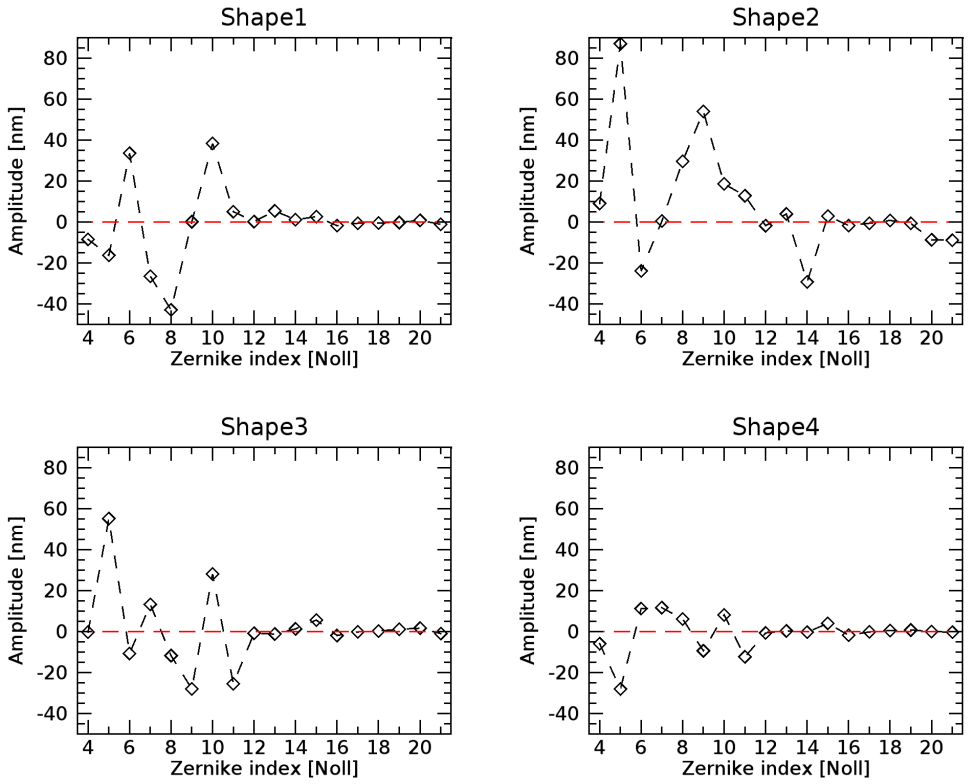

Figure 3. Zernike decompositions of the four shapes as measured by the Zygo.

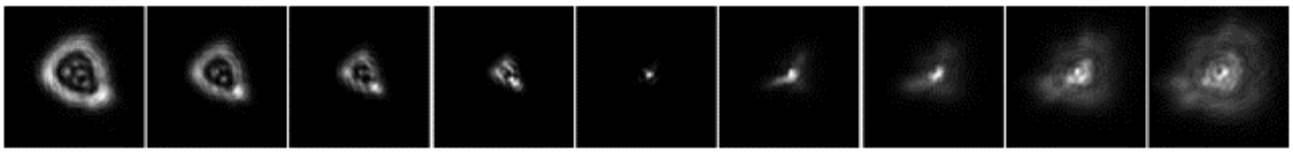

Figure 4. The complete sequence of Shape3 pre-processed unbinned images. From left to right: -2.5λ, -2λ, -1.5λ, -1λ, 0λ, $+1\lambda$, $+1.5\lambda$, $+2\lambda$, $+2.5\lambda$ peak-to-valley defocus (at 633nm).

5. ANALYSIS & RESULTS

5.1 CONVERGENCE RATE

As detailed in Section 3, we have at our disposal nine images at different positions of the camera along the optical axis (i.e. with different defocus amounts). In principle, we can run PD with any arbitrary combination of two or more of them. The amount of testable combinations of Nim images is given by the binomial coefficient C(9,Nim): 36 combinations with 2 images, 84 with 3 images, 126 with 4 images and so on, for a grand total of 502 combinations. It may happen that in some cases the algorithm gets trapped into local minima, giving a solution which is clearly wrong. This mainly happens when the number of images is small (say 2 or 3). Let's indicate the PD-reconstructed wavefront as $\vec{W}^{PD}$ (it is a vector of Zernike coefficients). We define the total differential wavefront error as the square sum of the residuals after subtraction of a reference measurement $\vec{W}^{ref}$:

$$\Delta WFE = \sqrt{\sum (\vec{W}^{PD} - \vec{W}^{ref})^2}$$

A convergence is when this error is smaller than a given threshold, given in percentage of the reference total wavefront error:

$$\Delta WFE < threshold \times \sqrt{\sum (\vec{W}^{ref})^2}$$

As for the reference, the two most logical choices are the Zygo measurement and the PD reconstruction using the whole set of 9 images (PD9, hereafter). As a first step of the analysis we are more interested in assessing the self-consistency of the reconstruction algorithm as we change combinations of input images, rather than looking at consistency with another independent measurement. For this reason we opted for PD9. For a comparative analysis between PD and Zygo please refer to Section 5.2.
We report in Table 1 and Table 2 the PD convergence rates as a function of the number of images, with no binning and binning 2x2, respectively. Convergence threshold is set to 0.1. Convergence rates are simply defined as the number of converging combinations over the total number of combinations. We can notice how the algorithm is systematically more likely to converge when we use three images or more, and this holds true in both binned and non-binned cases. Shape2 is the only notable exception to this trend, showing convergence rates not tending to 100% as the number of images increases. The difficulty in convergence in this case may be attributed to phase wrapping, being Shape2 peak-to-valley OPD larger than the sensing wavelength (see Figure 2). Finally, there is no clear evidence of one of the two binning modes being more robust than the other.

Table 1. PD convergence rates without binning as a function of the number of images used for reconstruction. Second column reports the number of possible combinations, given by the binomial coefficient C(9,Nim).

Nim	Ncombos	Shape1	Shape2	Shape3
2	36	0.42	0.61	0.36
3	84	0.83	0.79	0.73
4	126	0.95	0.79	0.91
5	126	0.99	0.71	0.97
6	84	1.00	0.71	1.00
7	36	1.00	0.53	1.00
8	9	1.00	0.78	1.00

Table 2. PD convergence rates with binning 2x2 as a function of the number of images used for reconstruction. Second column reports the number of possible combinations, given by the binomial coefficient C(9,Nim).

Nim	Ncombos	Shape1	Shape2	Shape3	Shape4
2	36	0.47	0.69	0.56	0.28
3	84	0.92	0.77	0.86	0.73
4	126	1.00	0.77	0.97	0.92
5	126	1.00	0.70	0.99	0.99
6	84	1.00	0.70	1.00	1.00
7	36	1.00	0.56	1.00	1.00
8	9	1.00	0.67	1.00	1.00

5.2 PHASE DIVERSITY vs ZYGO

In comparing PD and Zygo measurements we need to take into account NCPA between the two sensing channels. In fact, with flat DL we see a discrepancy between the two sensors amounting to 20nm overall (mainly coma). Moreover, some modes are measured with opposite signs by the two sensors. Calibration of the signs has been done empirically by pushing one mode at a time. As for NCPA, in order to eliminate them we subtracted the respective flats to all of the measurements we want to compare.
In Figure 5 we report the comparison between PD9 and Zygo for each of the 4 shapes. Binning is 2x2. Zygo data points are the average of the two interferograms (see Section 3). PD reconstructions match quite well with the Zygo measurements: residual wavefront errors are around 20% of the overall wavefront as measured by Zygo, with a worst case of 26% for Shape2. If we look mode by mode, the strongest discrepancies are in the defocus

term. This is due to the fact that radial modes suffer from higher reconstruction uncertainties.[5] Moreover, by looking at the interferograms we noticed that the DL drifts in focus in some cases. The strongest drift we found is in the interferograms with flat DL and it amounts to 40nm, while for the four shapes we found a maximum drift of 15nm. Such drifts occurring while PD images are acquired surely affect the reliability of defocus estimation. No other mode exhibits significant drifts. If we exclude defocus, the highest mismatch for three of the four shapes (with the only exception of Shape3) is in the mode having more power. For all of the shapes, the highest mismatches are almost always in the direction of PD measuring slightly higher amplitudes.

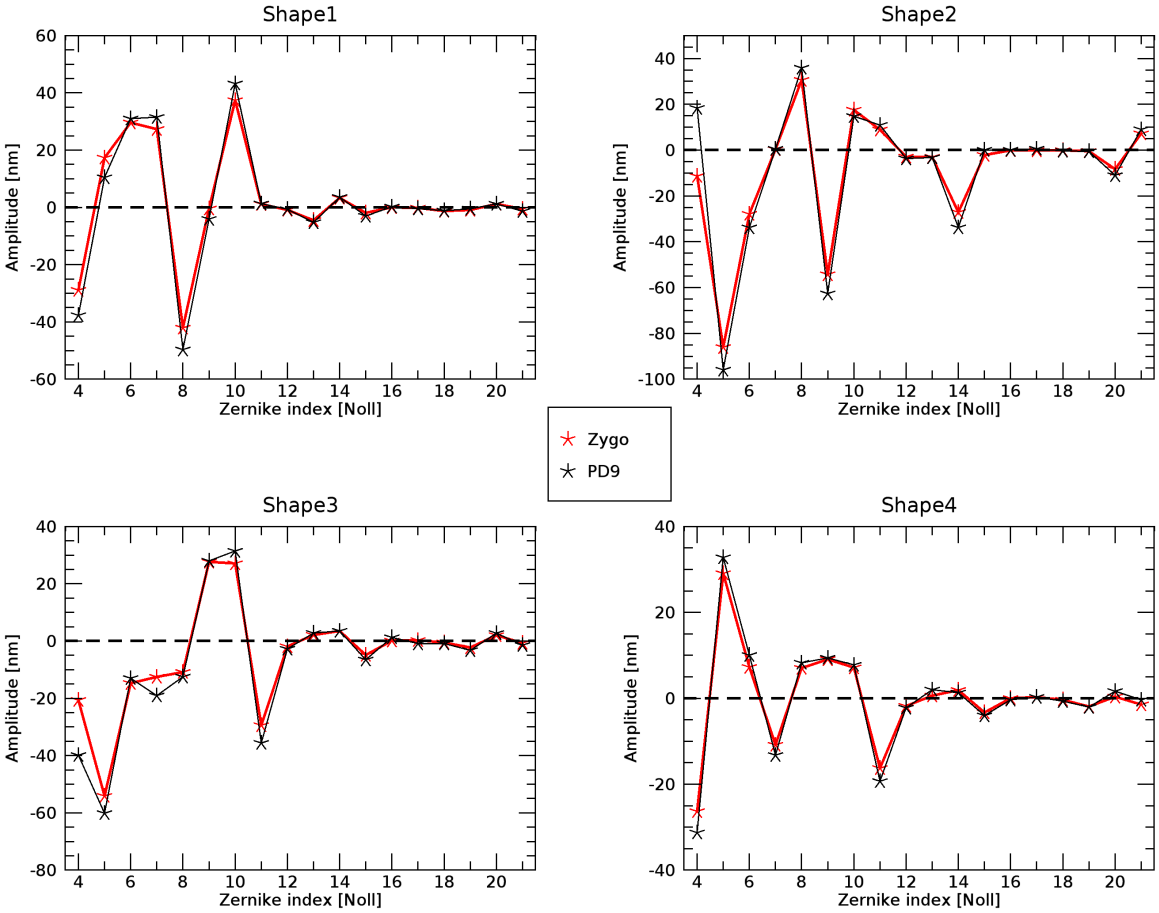

Figure 5. Comparison between phase diversity reconstruction using the whole set of nine images (PD9) and Zygo measurement, for each of the four shapes.

5.3 SHARK-LIKE PD

The original strategy for PD on SHARK-NIR was based on the acquisition of just two images. The instrument has two internal calibration fibers, one optically conjugated to the scientific camera and the other one a few millimeters after it so to introduce a defocus of -1λ ($1.6\mu m$). Using these two fibers we can sense the aberrations of the instrument bench alone. However, an external source is needed to sense the whole NCPA train (including the AO WFS path). In that case the baseline strategy consisted in using a defocussing lens in combination with the dual band imaging mode of SHARK-NIR. This lens introduces a defocus of $+2\lambda$ in just one of the two beams, allowing us to generate the in-focus and out-of-focus images at the same time. In both cases, however, the amount of defocus is fixed and cannot be tuned. The results of these new tests strongly suggest that just one intra/extra focal image is not enough to get a reliable and robust reconstruction: convergence rate with only two images is 0.5 on average. Moreover, if we restrict our statistics to the $(0\lambda,-1\lambda)$ combo alone, convergence rate calculated on the whole amount of DL shapes for which we have PD data (not only the four composite shapes,

but also single-mode aberrations used to characterize the DL) is as low as 20%. According to Table 2, if we exclude the highly aberrated Shape2 convergence is always above 90% with four or more defocus amounts. Four amounts can be considered as our lower limit. In order to reach it in SHARK-NIR, we decided to install two additional defocussing lenses. These two lenses introduce 2λ defocus in opposite directions and are placed in the first pupil plane filter wheel, being therefore insertable in the main optical path, only one of them at a time, just when needed. By combining them with the already in-place defocus sources, we will be able to reach up to six defocus amounts (in-focus case included) when operating with the internal fibers and four when operating with an external source in dual-band imaging mode. Specifically, the defocus we can inject in the first case ranges from -3λ to +2λ peak-to-valley at steps of 1λ, while in the second from -2λ to +4λ at steps of 2λ.
Established that using all of these four (or six) defocus amounts should guarantee convergence, it is interesting to look at convergence rates using subsets of them. It is important to point out here that the amount of time required to get a wavefront reconstruction with PD (images acquisition plus algorithm convergence time) grows with the number of images. This is a factor to take into account, especially in the perspective of night-time operations. Therefore, if one or more subsets come out to be robust enough, we might even consider using them instead of acquiring all of the available defocus amounts. With this in mind, we ran the same convergence analysis as in Section 5.1, this time considering only the defocus amounts that will be available on SHARK-NIR after the addition of the two defocussing lenses. However, not all of them are represented in the dataset analyzed in this work (we miss the -3λ and the +4λ). As for the internal sources configuration, we replaced the -3λ with the available -2.5λ. Concerning the external source configuration, we replaced the +4λ with the +2.5λ. Binning is 2x2, reference is PD9 and the convergence threshold is the same as in Section 5.1 Results are reported in Table 3. If we exclude Shape2, using four out of the six images available with the internal fibers should guarantee 100% convergence. On the other side, when running PD with an external source there is the indication that three images might not be enough stable when aberrations are small.

Table 3. PD convergence rates considering only those defocus combinations that will be available on SHARK-NIR after introduction of two additional defocussing lenses. On the left side, the case of PD with the internal fibers (six defocus amounts), while on the right side the case of PD with an external source (four defocus amounts).

Internal source				
Nim	Shape1	Shape2	Shape3	Shape4
2	0.40	0.67	0.60	0.33
3	0.90	0.75	0.95	0.75
4	1.00	0.53	1.00	1.00
5	1.00	0.67	1.00	1.00

External source				
Nim	Shape1	Shape2	Shape3	Shape4
2	0.50	0.67	0.67	0.33
3	1.00	1.00	1.00	0.50

5.4 CURVATURE-LIKE ANALYSIS

Having pairs of defocussed images equally spaced on both sides of the focal plane also offers the possibility to reconstruct the aberrations by measuring the wavefront local curvature. For the purpose, we used a software developed for LSST and publicly available on gitlab.[10] Wavefront reconstruction is modal and it is based on the method of Zernike polynomials series expansion by Gureyev et al.[11] In comparing this approach with Zygo the same considerations reported in Section 5.2 are valid, namely that flats are subtracted from both measurements and signs of individual modes are calibrated empirically. Image pre-processing doesn't change, except for the fact that now we have to make sure that intra and extra focal images are co-aligned. To do that, we used the differential tip/tilt estimated with PD (see Section 4).
With this curvature-like approach we are able to retrieve single-mode aberrations in quite an accurate way (errors of the order of 5-10nm maximum). However, with the four shapes the reconstructions are less accurate. In general, only the image pairs $\pm 1.233mm$ and $\pm 1.849mm$ give good results, while with higher defocus reconstructions significantly deviate from Zygo. In Figure 6 we report the comparison between Zygo and curvature-like estimation in the case of Shape3, which is the one giving the tightest match.

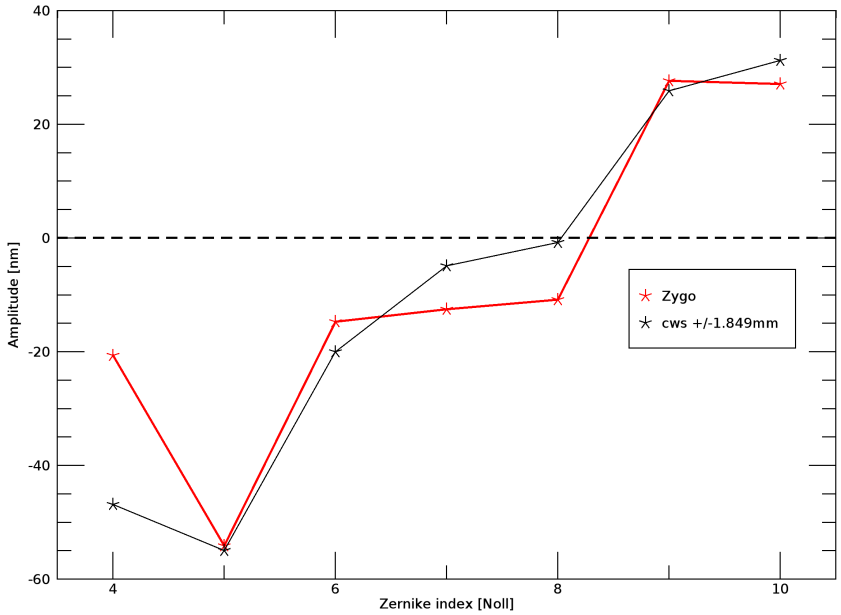

Figure 6. Comparison between Zygo and curvature-like estimation in the case of Shape3.

6. CONCLUSIONS

We presented new results of laboratory tests performed at INAF-Padua aimed at further characterizing phase diversity (PD) wavefront sensing for implementation in SHARK-NIR, the forthcoming LBT high-contrast imager. For the purpose, we built a new bench equipped with a Zygo interferometer, a deformable lens to inject aberrations and a camera mounted on a linear stage. The main result of this analysis is that PD highly benefits from using more than just one in-focus and one out-of-focus images, as it was originally foreseen for SHARK-NIR. Moreover, comparison with an independent wavefront measurement (Zygo) confirms the results of previous tests as for the reliability of wavefront estimation in laboratory conditions. These results led to the addition of two defocussing lenses inside the instrument. By combining these lenses with the already in-place defocus sources, we will be able to introduce up to six different defocus amounts (in-focus case included) when operating with the internal fibers and four when operating with an external source. In the first case, using just four out of the six available images should guarantee 100% convergence. On the other side, when running PD with an external source there is the indication that using less than four images might not be enough stable when aberrations to be corrected are small.

Finally, an alternative sensing using wavefront curvature has been devised. Results are preliminary and further work is needed to optimize the method.

REFERENCES

[1] Farinato, J., Baffa, C., Baruffolo, A., Bergomi, M., Carbonaro, L., Carlotti, A., Centrone, M., Codona, J., Dima, M., Esposito, S., Fantinel, D., Farisato, G., Gaessler, W., Giallongo, E., Greggio, D., Hinz, P., Lisi, F., Magrin, D., Marafatto, L., Pedichini, F., Pinna, E., Puglisi, A., Ragazzoni, R., Salasnich, B., Stangalini, M., Verinaud, C., and Viotto, V., "The NIR arm of SHARK: System for coronagraphy with High-order Adaptive optics from R to K bands," *International Journal of Astrobiology* **14**, 365–373 (2015).

[2] Farinato, J. et al., "SHARK-NIR, ready to "swim" in the LBT northern hemisphere "ocean"," *in these proceedings*.

[3] Martinez, P., Kasper, M., Costille, A., Sauvage, J.-F., Dohlen, K., Puget, P., and Beuzit, J. L., "Speckle temporal stability in xao coronagraphic images. ii. refine model for quasi-static speckle temporal evolution for VLT/SPHERE," *Astron. Astrophys.* **554**, A41 (2013).

[4] Gonsalves, R. A., "Phase retrieval and diversity in adaptive optics," *Optical Engineering* **21**, 829–832 (1982).

[5] Jolissaint, L., Mugnier, L. M., Neyman, C., Christou, J., and Wizinowich, P., "Retrieving the telescope and instrument static wavefront aberration with a phase diversity procedure using on-sky adaptive optics corrected images," *Proc. SPIE* **8447**, 844716 (2012).

[6] Vassallo, D., Farinato, J., Sauvage, J.-F., Fusco, T., Greggio, D., Carolo, E., Viotto, V., Bergomi, M., Marafatto, L., Baruffolo, A., and Marco, D. P., "Validating the phase diversity approach for sensing NCPA in SHARK-NIR, the second-generation high-contrast imager for the large binocular telescope," in [*Modeling, Systems Engineering, and Project Management for Astronomy VIII*], *Proc. SPIE* **10705** (2018).

[7] Vassallo, D., Bergomi, M., Biondi, F., Carolo, E., Greggio, D., Marafatto, L., Umbriaco, G., Baruffolo, A., Marco, D. P., Plenz, M., Radhakrishnan, K., Viotto, V., Sauvage, J.-F., Fusco, T., and Farinato, J., "Laboratory demonstration of focal plane wavefront sensing using phase diversity: a way to tackle the problem of NCPA in SHARK-NIR," in [*Ground-based and Airborne Instrumentation for Astronomy VIII*], *Proc. SPIE* **11447** (2020).

[8] Gabriele, U. et al., "Deformable lens for testing the performance of focal-plane wavefront sensing using phase diversity," *in these proceedings*.

[9] Sauvage, J.-F., Fusco, T., Rousset, G., and Petit, C., "Calibration and precompensation of noncommon path aberrations for extreme adaptive optics," *Journal of the Optical Society of America A* **24**, 2334 (2007).

[10] Xin, B., Claver, C., Liang, M., Chandrasekharan, S., Angeli, G., and Shipsey, I., "Curvature wavefront sensing for the large synoptic survey telescope," *Applied Optics* **54**, 9045–9054 (2015).

[11] Gureyev, T. E., Roberts, A., and Nugent, K. A., "Phase retrieval with the transport-of-intensity equation: matrix solution with use of zernike polynomials," *Journal of the Optical Society of America A: Optics, Image Science, and Vision* **12**(9), 1932–1941 (1995).